Automotive Experiences
Vol. 9 No. 1 (2026) pp. 204-222
p-ISSN: 2615-6202 e-ISSN: 2615-6636

Research Paper

Probabilistic Performance Prediction of a Hydrogen-Converted SI Engine Using a Markov-Chain-Wiebe Framework

Purnami[1], **Willy Satrio Nugroho**[1], **Lilis Yuliati**[1], **Fikrul Akbar Alamsyah**[1], **Abdul Mudjib Sulaiman Wahid**[2], **I Nyoman Gede Wardana**[1]

[1]Department of Mechanical Engineering, Brawijaya University, Malang 65145, Indonesia
[2]School of Mechanical and Aerospace Engineering, Nanyang Technological University, 639798, Singapore

purnami.ftub@ub.ac.id

https://doi.org/10.31603/ae.15544

Published by Automotive Laboratory of Universitas Muhammadiyah Magelang

Article Info
Submitted:
09/12/2025
Revised:
11/04/2026
Accepted:
14/05/2026
Online first:
14/05/2026

Abstract

This study employs a novel Markov-chain modeling framework to analyze the combustion-performance interaction in a hydrogen-fueled spark-ignition engine. The methodology integrates a Wiebe heat-release model within a Markov-chain state-transition framework, where each discrete engine state defines combustion parameters and probabilistic transitions capture cycle-to-cycle variability. Results demonstrate that engine behavior is dominantly governed by combustion phasing, with spark timing exerting primary control over torque, efficiency, and brake-specific fuel consumption (BSFC). Sensitivity analysis confirms spark timing produces the steepest performance gradients, while ignition voltage offers secondary benefits and engine speed exhibits minimal influence. The model reveals a highly nonlinear torque response to spark advance, characterized by a rapid rise culminating in a narrow maximum brake torque (MBT) plateau at 8°–10° BTDC, corresponding to a distinct BSFC minimum. Significant data scatter underscores the stochastic nature of hydrogen combustion, arising from multidomain interactions between air-fuel ratio, ignition strength, and phasing. The Markov-chain approach successfully captures this coupled deterministic-probabilistic behavior, highlighting the critical need for precise spark-timing control to optimize performance in hydrogen applications.

Keywords: Hydrogen internal combustion engine; Combustion phasing; Spark ignition; Markov-chain; Performance prediction

1. Introduction

Hydrogen is increasingly recognized as a viable carbon-free energy carrier for next-generation propulsion systems, particularly for spark-ignition (SI) internal combustion engines (ICEs). Its high diffusivity, wide flammability limits, and exceptional flame speed allow stable combustion even under ultra-lean conditions, enabling high efficiency and near-zero carbon emissions [1]. When combusted, hydrogen produces only water vapor as its primary product, eliminating CO_2 and most hydrocarbon-based pollutants [2]. However, hydrogen classified based on its carbon footprint into several spectrum of colors [3]. The cleanest hydrogen is only green hydrogen generated from renewable electricity sourced water electrolysis [4]. Therefore, green hydrogen is the most suitable future fuel to support net zero emission (NZE) 2050 target as stated in Paris agreement [5]. As a result, this motivates global research on adapting existing ICE platforms to operate cleanly using hydrogen while leveraging current manufacturing infrastructure.

Despite these advantages, hydrogen combustion introduces unique technical challenges. The high adiabatic flame temperature and rapid reaction kinetics can increase NO_x formation, while its low ignition energy raises susceptibility to pre-ignition, backfire, and abnormal combustion [6]. Additionally, hydrogen low volumetric energy density and distinct auto-ignition characteristics complicate mixture preparation and spark control strategies [7]. These issues highlight the need for advanced modeling frameworks that can capture the complex interactions among ignition timing, equivalence ratio, mixture thermodynamics, and combustion phasing.

Hydrogen unique physicochemical properties originate from its molecular simplicity and low molecular weight. Thise results in an exceptionally high binary diffusion coefficient in air (on the order of 0.6-0.8 cm^2/s at ambient conditions) which enables rapid mixing and homogeneous charge formation [8]. In addition, hydrogen exhibits a high laminar flame speed (typically 2-3 m/s under stoichiometric conditions), driven by fast chain-branching reactions involving H, O, and OH radicals which accelerate combustion kinetics [9]. Furthermore, its extremely low minimum ignition energy (~0.02 mJ) is associated with efficient radical generation even under weak spark conditions. Hence, allows reliable ignition in ultra-lean mixtures [10]. These molecular-level characteristics collectively enable stable combustion over a wide flammability range (4-75% by volume in air) making hydrogen attractive for highly efficient and lean-burn engine operation [11].

Significant progress has been made in hydrogen combustion modeling, especially through zero-dimensional (0-D) and phenomenological models based on Wiebe heat-release functions, laminar-flame correlations, and empirical ignition characteristics [12]. Such deterministic models accurately capture average engine behavior; however, they often fail to represent cycle-to-cycle variability, stochastic mixture fluctuations, or probabilistic ignition events phenomena that become more pronounced at lean conditions and low ignition energy [13]. Therefore, deterministic approaches alone remain insufficient for capturing the full spectrum of hydrogen combustion behavior.

To address such limitations, stochastic and probabilistic modeling frameworks have gained attention. Markov-chain-based formulations, in particular, offer a capability to represent transitions between discrete engine operating states defined by parameters such as speed, equivalence ratio, spark timing, and ignition voltage [14]. These models permit analysis of expected long-term behavior as well as cycle-to-cycle variations in heat release, peak pressure, and combustion stability [15]. Despite their promise, the application of Markov-chain approaches to hydrogen-fueled SI engines remains limited in the literature.

Recent studies have emphasized the importance of incorporating probabilistic modeling and uncertainty quantification in combustion simulations to account for inherent uncertainties in thermochemical processes and flow dynamics [16]. In parallel, data-driven stochastic approaches combined with Markov-based frameworks have demonstrated strong capability in capturing transient combustion modes and probabilistic state transitions in complex combustion systems [17]. Furthermore, combustion variability has been identified as a critical issue in hydrogen-fueled engines, where small fluctuations in fuel composition and operating conditions can significantly influence flame stability, heat-release characteristics, and cycle-to-cycle variations [18]. Experimental investigations on hydrogen SI engines also confirm that cyclic dispersion in pressure and combustion phasing plays a key role in determining stable engine operation [19]. Although hydrogen ICE modeling has been extensively studied using deterministic thermodynamic and kinetic approaches [20], [21], the integration of stochastic combustion variability and probabilistic modeling into a unified predictive framework remains limited. This highlights a clear research gap in developing models that simultaneously capture deterministic performance trends and stochastic combustion behavior in hydrogen-fueled engines.

In parallel, regional investigations have provided important exploratory findings relevant to hydrogen-adapted engines. For example, previous studies have reported hydrogen-assisted combustion behaviors under locally modified engine configurations [22]. These findings, though limited in scale, underscore both the feasibility and the technical challenges associated with hydrogen implementation in practical engines. Key hurdles include managing hydrogen high flame speed and low ignition energy to prevent abnormal combustion, optimizing air-fuel ratio within a narrow window for efficiency while avoiding NOx penalties, and designing control systems robust enough to handle its heightened sensitivity to mixture preparation and cycle-to-cycle variation [23], [24]. This reinforces the need for robust, flexible modeling tools capable of navigating this complex parameter space.

This study addresses these gaps by proposing a Markov-Chain-Based Combustion Modeling framework integrated with a Wiebe-type heat-release formulation. The model evaluates a wide parameter space including engine speed, equivalence ratio, spark timing, ignition voltage, and combustion duration to predict torque, efficiency, pressure evolution, heat-release rate, and temperature traces. By combining deterministic thermodynamic modeling with a probabilistic state-transition system, this approach provides a digital-twin-like simulation environment capable of representing both idealized and stochastic combustion behavior in hydrogen-fueled SI engines.

2. Methods

2.1. *Engine Model Configuration*

The engine evaluated in this study is a four-stroke spark-ignition engine originally designed for gasoline but virtually modified to operate with hydrogen fuel. The model setup is shown in **Figure 1** and the complete parameters were listed in **Table 1**. The numerical model assumes a homogeneous hydrogen–air mixture entering the cylinder, a fixed geometric compression ratio (CR), and conventional crank-slider kinematics for volume evaluation. The operating parameters selected for analysis include engine speed (RPM), equivalence ratio (λ), spark timing (°CA BTDC), and ignition voltage (kV). These four parameters constitute a multidimensional operating domain, and their values are discretized to form the state space of the Markov chain.

The main geometric and operating specifications of the baseline engine used in this study are summarized in **Table 1**. These parameters define the thermodynamic boundary conditions and are required to ensure reproducibility of the model [25], [26]. The selected specifications are representative of a small-scale spark-ignition engine and tare kept constant throughout the simulations unless otherwise stated.

The hydrogen fuel was modeled under the assumption of ideal gas behavior, and its combustion characteristics namely, rapid flame speed and low ignition energy-are incorporated through the selection of Wiebe parameters that differ from gasoline values. The Wiebe function represents the entire combustion process in a lumped manner, where flame development and late combustion effects are implicitly included within the burn-rate parameters. The overall approach enables the representation of the unique thermochemical properties of hydrogen while preserving the underlying structure of the gasoline engine framework.

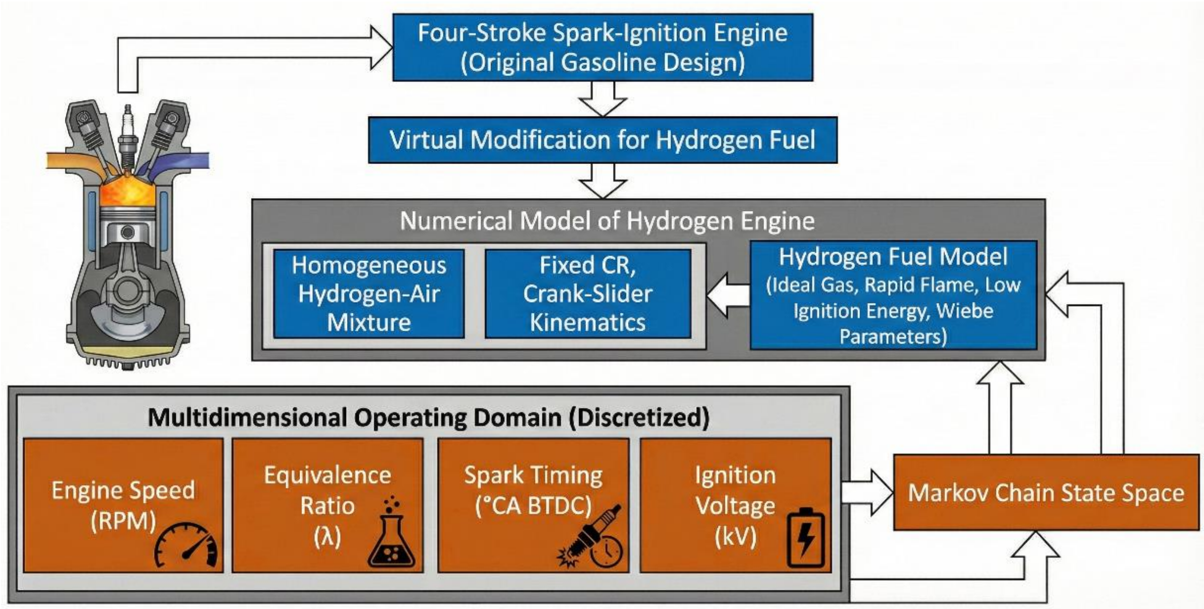

Figure 1. State transition matrix diagram for hydrogen ICE Markov model

Table 1. Fuels properties

Parameter	Symbol	Value
Engine type	–	4-stroke SI engine
Number of cylinders	–	1
Bore	B	68 mm
Stroke	S	54 mm
Displacement volume	Vd	196 cc
Compression ratio	CR	8.5:1
Connecting rod length	L	110 mm
Fuel type	–	Hydrogen (converted from gasoline)
Lower heating value	Q_LHV	120 MJ/kg
Intake pressure	Pin	1 atm
Intake temperature	Tin	300 K
Engine speed range	RPM	1000–4000 rpm
Equivalence ratio range	λ	0.6–1.2
Spark timing range	θspark	0–20° BTDC
Ignition voltage range	Vspark	8–12 kV

The hydrogen fuel was modeled under the assumption of ideal gas behavior, and its combustion characteristics namely, rapid flame speed and low ignition energy-are incorporated through the selection of Wiebe parameters that differ from gasoline values. The Wiebe function represents the entire combustion process in a lumped manner, where flame development and late combustion effects are implicitly included within the burn-rate parameters. The overall approach enables the representation of the unique thermochemical properties of hydrogen while preserving the underlying structure of the gasoline engine framework.

2.2. *Engine State Definition for Markov Chain*

To represent the natural variability of engine operating conditions, each unique combination of engine speed, equivalence ratio, spark timing, and ignition voltage was treated as a discrete state in a first-order Markov chain. If a state is denoted as Eq. (1) [27].

$$Xt = \{RPMt, \lambda t, \theta spark, t, Vspark, t\} \quad (1)$$

Then the probability of transitioning to a future state X_{t+1} depends only on the current state, consistent with the Markov property shown in Eq. (2) [28].

$$P(Xt + 1 \mid Xt, Xt - 1, \dots) = P(Xt + 1 \mid Xt) \quad (2)$$

Each parameter is assigned a transition probability determining whether its value remains constant or shifts to an adjacent bin. For example, if the equivalence ratio consists of bins $\lambda_1, \lambda_2, \dots, \lambda_n$, the transition probability from λ_i to λ_{i+1} or λ_{i-1} was defined such that small incremental changes dominate, mimicking realistic engine behavior. The complete transition matrix was constructed as the Kronecker product of the four individual parameter transition matrices [29]. This ensures that the Markov chain explores the operating map gradually but stochastically.

2.3. *Cylinder Volume Modeling*

The instantaneous cylinder volume is calculated using a standard geometric model of the piston-crank mechanism. For a crank angle θ, the cylinder volume is expressed as in Eq. (3) [30]. Where V_c is the clearance volume, B is the cylinder bore, S is the stroke, and L is the connecting rod length. This formulation captures the compression and expansion processes accurately and is used to compute the pressure-volume work over the cycle.

2.4. *Cylinder Volume Modeling*

Combustion at each Markov state was modeled using a single-zone, zero-dimensional energy conservation framework. The mass fraction burned $x_b(\theta)$ was described using the classical Wiebe function in Eq. (4) [31].

Where a is the combustion efficiency shaping factor, m is the form factor controlling the burn rate profile, θ_0 is the start of combustion, and $\Delta\theta$ is the combustion duration. In this formulation, the parameter a determines the completeness of combustion (typically $a \approx 5$–6 for near-complete combustion), while m controls the shape of the heat-release curve, with higher values producing

$$V(\theta) = V_c + \frac{\pi B^2}{4}[S + \frac{S}{2}(1 - \cos\theta) + (L - \sqrt{L^2 - (S/2\sin\theta)^2})] \quad (3)$$

a steeper and more rapid combustion process. The start of combustion θ_0 is defined by the spark timing, and the combustion duration $\Delta\theta$represents the crank-angle interval over which 0–99% of the fuel is burned. Differentiation provides the heat release rate as modelled with Eq. (5).

$$x_b(\theta) = 1 - \exp[-a(\frac{\theta - \theta_0}{\Delta\theta})^{m+1}] \quad (4)$$

$$\frac{dQ}{d\theta} = Q_{\text{LHV}}\frac{dx_b}{d\theta} \quad (5)$$

With Q_{LHV} represents the lower heating value of hydrogen, multiplied by the mass of fuel injected into the cylinder. In this study, representative Wiebe parameters for hydrogen combustion were selected as $a = 5$, $m = 2$–3, and $\Delta\theta = 20°$–$40°$CA, reflecting the faster combustion characteristics of hydrogen compared to conventional gasoline engines. The parameter values were chosen based on typical ranges reported in hydrogen combustion literature and were kept consistent across all simulated states unless otherwise specified. Hydrogen's rapid burning behavior is represented by selecting a relatively small $\Delta\theta$and Hydrogen's rapid burning behavior is represented by selecting a relatively small $\Delta\theta$and higher m, resulting in a steep heat-release curve aligned with experimental characteristics of hydrogen ignition.

2.5. *Thermodynamic Model of Pressure and Temperature*

The first law of thermodynamics for an open system is used to compute the temperature and pressure evolution during the cycle. The energy equation in differential form was expressed in Eq. (6) [32].

$$\frac{dQ}{d\theta} = mc_v\frac{dT}{d\theta} + p\frac{dV}{d\theta} \quad (6)$$

where m is the mass of the mixture, c_v is the specific heat at constant volume, T is temperature, and p is pressure. Rearranging for temperature yields using Eq. (7) [32].

$$\frac{dT}{d\theta} = \frac{1}{mc_v}(\frac{dQ}{d\theta} - p\frac{dV}{d\theta}) \quad (7)$$

Pressure is then calculated using the ideal-gas relation shown in Eq. (8) [33].

$$p(\theta) = \frac{mRT(\theta)}{V(\theta)} \quad (8)$$

Where R is the specific gas constant, this system of equations was solved numerically along the crank-angle domain, producing the complete temperature trace, pressure trace, and heat-release profile for each simulated state.

In this study, a simplified thermodynamic model is adopted in which heat transfer losses, blow-by, and crevice effects are neglected to reduce computational complexity and focus on the dominant influence of combustion phasing and stochastic variability [34]. This assumption is reasonable for comparative analysis across operating conditions, although it may lead to slight overprediction of peak pressure and efficiency.

Additionally, the specific heat is assumed constant for simplicity; however, in reality, it varies with temperature and mixture composition [35]. Incorporating variable specific heat would improve thermodynamic accuracy but is beyond the scope of the present probabilistic framework.

2.6. *Estimation of Work, Fuel Consumption, and Efficiency*

The indicated work for a single cycle was computed by integrating the pressure over the volume trajectory as in Eq. (9) [36].

$$W = \oint p\, dV \quad (9)$$

From this, the indicated mean effective pressure (IMEP) is calculated using Eq. (10) [37], [38].

$$\text{IMEP} = \frac{W}{V_d} \quad (10)$$

Where $V_d$is the displaced volume. The indicated thermal efficiency follows from Eq. (11) [39].

$$\eta = \frac{W}{m_f Q_{\text{LHV}}} \quad (11)$$

While the brake specific fuel consumption (BSFC) was estimated using Eq. (12) [40].

$$\text{BSFC} = \frac{\dot{m}_f}{P_b} \quad (12)$$

With $P_b$the brake power assumed that mechanical losses may be incorporated in later extensions of the model. Outputs including $p(\theta)$, $T(\theta)$, HRR, and cumulative work trace $W(\theta)$ are stored for each Markov chain state.

2.7. *The Development of Markov Chain Model*

To construct discrete engine states for the Markov chain, four influential parameters were selected Engine speed (RPM), Excess-air ratio (λ), Spark timing (ST), Spark voltage (SV). Each parameter was discretized into a specified number of bins (4 RPM bins, 4 λ bins, 3 spark timings, and 3 voltage levels), generating a state space with Eq. (13) [41]. The discretization balances simulation coverage and computational tractability while adequately representing hydrogen sensitivity to ignition energy, mixture strength, and flame speed [42].

$$N = n_{RPM} \cdot n_{\lambda} \cdot n_{ST} \cdot n_{SV} \tag{13}$$

State evolution was modeled as a time-homogeneous Markov chain where each state transition is governed by Eq. (14) [43].

$$P(Xk + 1 = j \mid Xk = i) = Pij \tag{14}$$

Diagonal entries represent a "stay probability," whereas off-diagonal entries correspond to transitions into neighboring states. Specifically, the stay probability is defined as $P_{ii} = p_s$, where $p_s \in [0,1]$represents the probability that a parameter remains in the same discrete state between two consecutive steps. The transition probability to a different state $j \neq i$is defined as $P_{ij} = (1 - p_s)/N_i$, where N_i is the number of allowable neighboring states. For example, RPM is allowed to transition only to the same bin or an adjacent bin, reflecting mechanical inertia. Mixture ratio, spark timing, and spark voltage transitions use similar localized transition rules. The transition matrix is row-stochastic and ensures valid probabilistic evolution across cycles [44]. The state transition diagram in **Figure 2** shows the Markov structure used to model hydrogen ICE behavior.

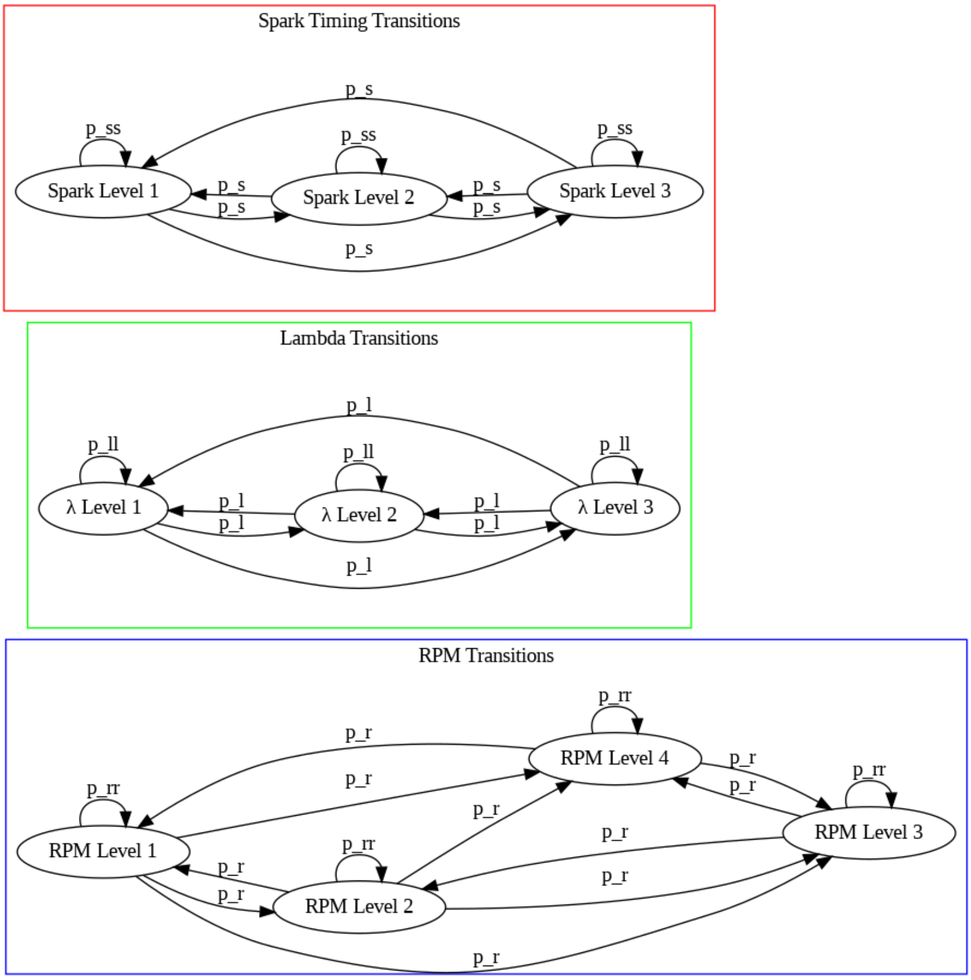

Figure 2. Markov structure used to model hydrogen ICE behavior

Each engine state was defined as a triplet (r_i, λ_j, s_k), where r_i is the discrete engine speed level (RPM Level 1-4), λ_j denotes the air–fuel equivalence ratio levels (λ Level 1-3), and s_k represents the spark timing levels (Spark Level 1-3) (see **Figure 2**). These discrete levels are generated directly from the simulation grid: for RPM, the range $[rpm_{\min}, rpm_{\max}]$ was divided into four bins; for λ, the interval $[\lambda_{\min}, \lambda_{\max}]$ was divided into three bins; and similarly three bins are created for the spark timing interval $[spark_{\min}, spark_{\max}]$. The diagram separates transitions for each dimension to clearly show their independent Markov behavior. For each parameter, a probability of staying in the same level is defined - p_{rr} for RPM, $p_{ll}$for λ, and p_{ss} for spark timingwhile the probability of transitioning to any other level of the same parameter (p_r, p_l, p_s) was evenly distributed among the remaining bins.

For each parameter, a probability of staying in the same level is defined as $p_{rr}$for RPM, $p_{ll}$for λ, and $p_{ss}$for spark timing, which correspond to the stay probabilities P_{ii}in each respective transition matrix. The probabilities of transitioning to neighboring states (p_r, p_l, p_s) are distributed according to $(1{-}p_{ii})$and normalized such that the sum of each row equals unity.

The full transition probability for moving from one engine state to another was computed as the product of Eq. (15). reflecting the independence of RPM, λ, and spark components in the Markov process. **Figure 2** visualizes this structure by showing self-loops for staying in the same level and bidirectional arrows between adjacent or non-adjacent levels representing allowed transitions with nonzero probability. The state-transition architecture forms the basis of the Markov chain used to explore the engine's performance landscape across all combinations of RPM, λ, and spark timing.

$$P((ri, \lambda j, sk) \to (ri', \lambda j', sk')) = pr(i \to i')p\lambda(j \to j')ps(k \to k') \tag{15}$$

3. Results and Discussion

Engine performance within this study is governed far more by combustion phasing than by mechanical operating speed, and this hierarchy of influence is clearly reflected in the comparative sensitivity of the three control parameters as visualized in **Figure 3**. Spark Timing emerges as the dominant factor, producing the largest and most consistent impact on torque, efficiency, and fuel consumption, as indicated by its substantially taller bar relative to the others. Ignition Voltage provides a secondary but meaningful contribution by strengthening the ignition process and improving combustion stability, though its overall effect remains noticeably smaller than that of Spark Timing. RPM contributes the least, with only minor variations in performance across the tested range, showing that engine speed plays a limited role when combustion parameters are varied simultaneously. Collectively, this pattern confirms that optimizing combustion timing is the

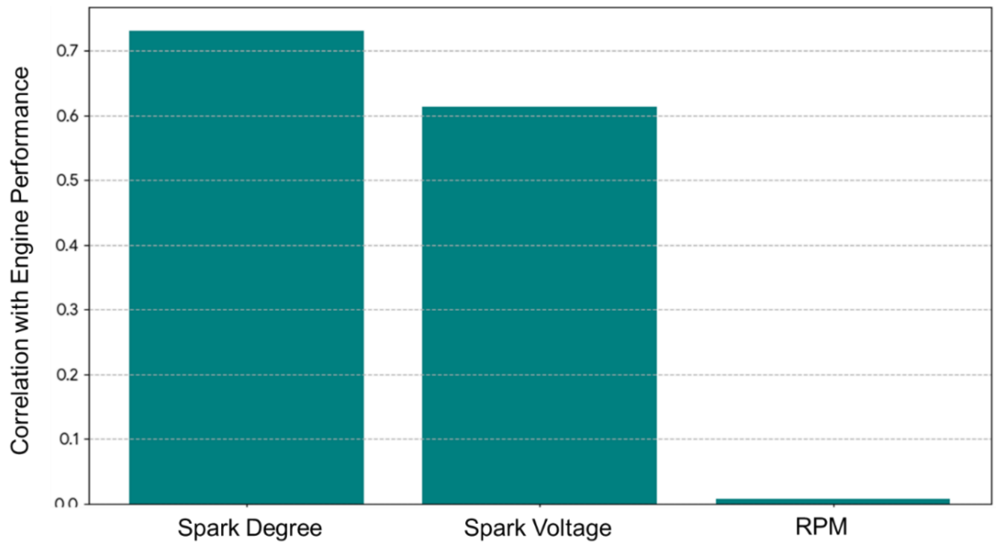

Figure 3. The parameter influence rank on overall engine performance

most critical lever for improving engine performance, followed by ignition strength, while RPM exerts only marginal influence under the studied conditions.

Figure 4 illustrates the cubic interpolation of engine torque as a function of spark timing and reveals a clear non-linear relationship between these two variables. The fitted cubic curve highlights the strong sensitivity of torque to spark advance in the early region: as spark timing increases from 0° to approximately 8°, torque rises sharply from about 12.5 Nm to around 14.4 Nm. This reflects the improved combustion phasing that occurs when the ignition event is advanced toward the optimal crank-angle position for maximum cylinder pressure [45] . The curve then transitions into a plateau region between 8° and 10°, where torque reaches its peak value of roughly 14.5 Nm. This zone corresponds to the Minimum advance for MBT, where further spark advancement produces negligible improvements and the combustion process is already near its optimal phasing [46]. This behavior indicates that once the peak pressure is optimally aligned near TDC, further advancement leads to diminishing returns due to increased negative work during compression.

The scatter points in **Figure 4** represent the raw simulation outputs and show noticeable vertical dispersion at each spark timing setting. For instance, at 8°, torque values range from approximately 14.0 Nm to 14.9 Nm. This spread is expected given the multidimensional nature of the input space, where torque is simultaneously influenced by engine speed (RPM), air–fuel ratio (λ), and ignition voltage (SV). Variations in these parameters shift the combustion conditions for a fixed spark timing value, producing the observed spread around the fitted curve. Overall, the results confirm that spark timing has a dominant and highly nonlinear influence on torque, and the cubic interpolation effectively captures both the peak region and the underlying variability driven by interacting engine parameters. This variability reflects the inherent sensitivity of hydrogen combustion to small perturbations in mixture composition and ignition conditions, which affect flame development and pressure rise rate.

The relationship between spark timing and fuel efficiency is clearly defined by the characteristic valley-shaped trend shown in **Figure 5**, where the red cubic-polynomial curve captures the strong nonlinear response of BSFC to combustion phasing. As the spark is advanced from 0° toward roughly 8° BTDC, BSFC decreases sharply, indicating a rapid improvement in fuel economy as the combustion event becomes better aligned with the point where peak cylinder pressure can deliver maximum useful work. A narrow optimum region appears between approximately 8° and 10° BTDC, where BSFC reaches its minimum and the engine achieves its highest fuel efficiency. Advancing the spark beyond this range reverses the trend, causing BSFC to rise again due to excessively early peak pressure and associated pumping and heat-loss

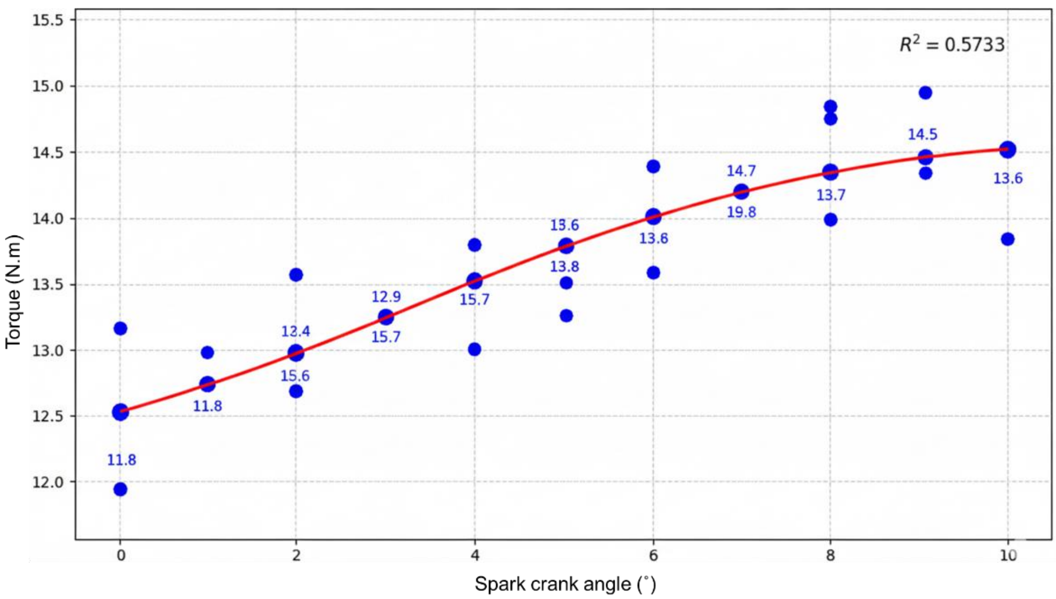

Figure 4. The influence of spark at certain crank angle on engine torque

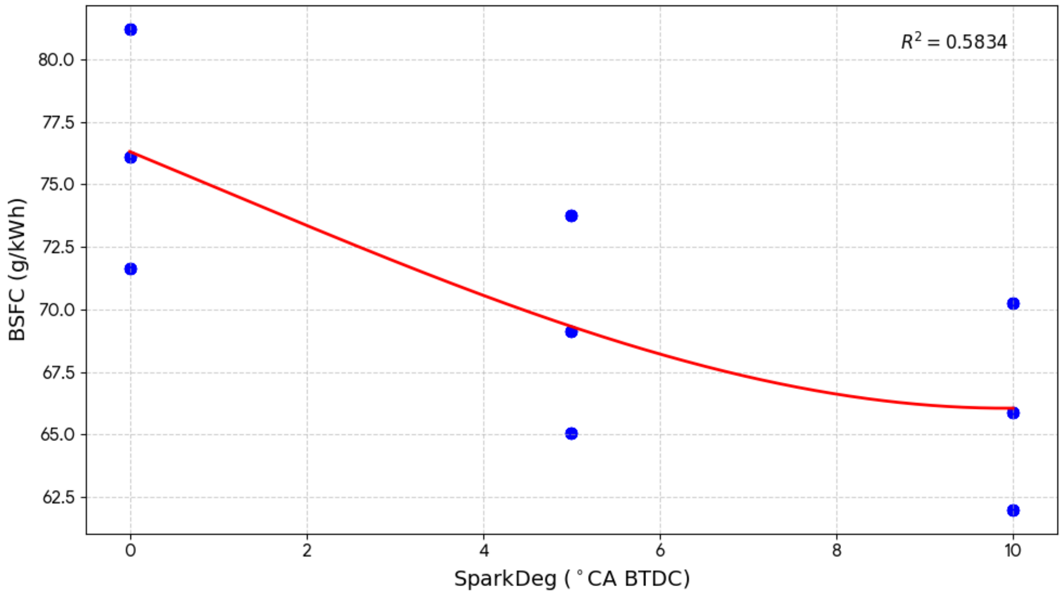

Figure 5. The influence of spark at certain crank angle on brake specific fuel consumption

penalties. Notably, this minimum in BSFC occurs in the same spark-timing window where torque reaches its maximum, confirming that both performance and efficiency are simultaneously optimized near 9° BTDC [47]. The scatter of individual data points around the fitted curve indicates that although spark timing exerts primary control over BSFC, secondary parameters such as ignition voltage, engine speed, and equivalence ratio still modulate the final efficiency outcome within the multidimensional simulation space. This alignment between torque peak and BSFC minimum confirms the classical MBT condition, where optimal combustion phasing maximizes energy conversion efficiency.

The dominant influence of spark timing observed in this study can be directly attributed to its control over combustion phasing and pressure peak alignment within the engine cycle. Specifically, advancing the spark timing shifts the start of combustion earlier, thereby controlling the crank-angle location of the peak cylinder pressure. Optimal performance is achieved when this pressure peak occurs slightly after TDC maximizing the effective expansion work while minimizing negative compression work [48], [49]. Therefore, spark timing simultaneously governs both the combustion phasing and the alignment of peak pressure, which explains its primary influence on torque, efficiency, and fuel consumption. In contrast, parameters such as ignition voltage mainly affect early flame kernel development, and engine speed influences the available time for combustion, making their impact comparatively secondary.

The relationship between ignition strength and combustion performance is illustrated by the efficiency response to variations in spark voltage (**Figure 6**). In this context, spark voltage primarily influences the initial flame kernel formation, where higher ignition energy enhances the probability of successful ignition and stabilizes early flame development, particularly under lean or marginal conditions. However, once a stable flame kernel is established, the subsequent combustion process is governed more strongly by mixture properties and combustion phasing, which explains the relatively weak sensitivity of efficiency to spark voltage. In general, increasing the spark voltage from 10.0 to 12.0 kV produces a mild upward trend in efficiency, indicating that a stronger ignition pulse contributes to slightly improved combustion stability and energy conversion. This trend is represented by the fitted red regression line; however, the underlying data exhibit substantial vertical scatter, demonstrating that efficiency is highly sensitive to additional operating variables beyond spark voltage alone. The moderate coefficient of determination (R^2 = 0.4252) confirms that only about 42% of the observed variation in efficiency can be attributed to changes in spark voltage, while the majority of the variability arises from interacting parameters such as air–fuel ratio, engine speed, and ignition

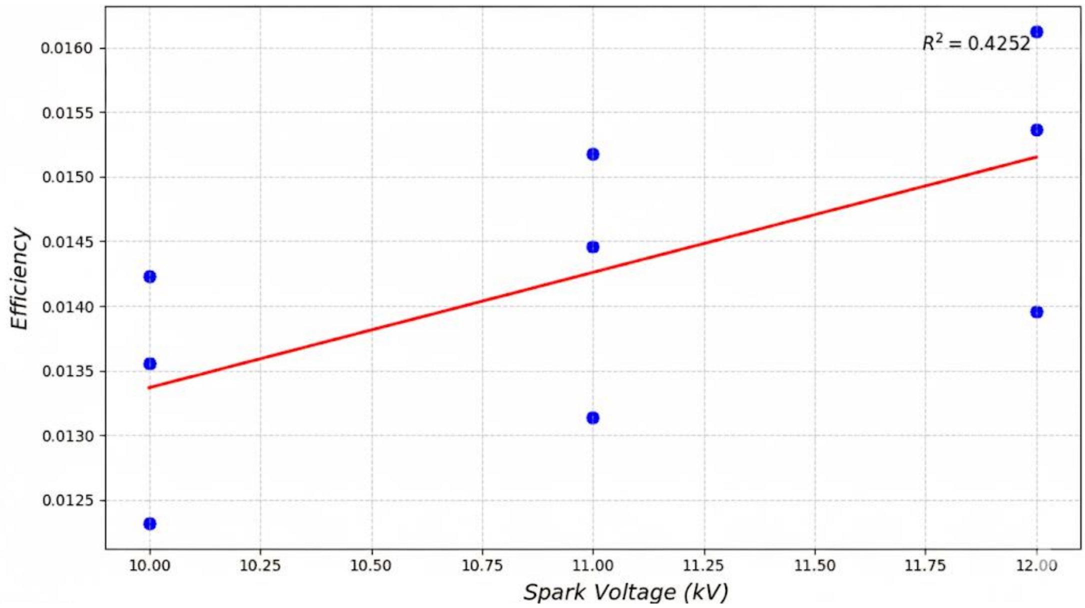

Figure 6. The influence of spark voltage for ignition on engine efficiency

timing. Thus, although higher spark voltage provides a measurable benefit, its influence is comparatively weak and inconsistent across the tested domain [50]. These indicates spark voltage acts as a secondary contributor to efficiency. The spark voltage effect was overshadowed by more dominant combustion-control variables such as spark degree. This suggests that once a stable ignition kernel is established, subsequent combustion is predominantly governed by mixture properties and flame propagation dynamics rather than ignition energy.

The heatmap in **Figure 7** provides a clear multidimensional visualization of how spark timing and air–fuel ratio jointly influence torque production, transforming the previously scattered data into a structured map of engine behavior. A distinct performance island emerges around 8°–10° BTDC and $\lambda \approx 1.0$, representing the MBT region where combustion phasing is optimally aligned with piston motion [51]. The strong horizontal color gradient confirms that spark timing is the dominant control parameter: advancing the spark rapidly increases torque as the high flame speed of hydrogen enables the pressure peak to occur just after TDC. In contrast, the vertical gradient shows that variations in λmodulate torque more gradually, with the sweet spot narrowing at lean or rich mixtures due to reduced energy density or altered flame-speed characteristics. Notably, the position of the optimal zone shifts slightly with changes in λ, indicating an interaction between mixture strength and required spark advance. This coupling effect demonstrates that spark timing and air–fuel ratio cannot be tuned independently and validates the model's ability to capture high-order, multivariable dependencies in hydrogen combustion behavior. This narrow high-performance region indicates that hydrogen combustion exhibits strong sensitivity to both phasing and mixture strength, requiring precise control to maintain optimal conditions.

Figure 8 presents the Probability Density Function (PDF) of torque across varying spark-timing settings, revealing how combustion phasing governs both the average performance and the statistical stability of the hydrogen-fueled engine. A distinct rightward shift in the distributions is observed as spark timing advances from 0° to 10° BTDC, indicating a continuous increase in mean torque and confirming that ignition phasing is the dominant control variable in determining work output [52]. The separation between the distribution peaks demonstrates that each spark-timing setting forms a unique performance regime, consistent with classical MBT behavior in hydrogen combustion [53]. The spread (width) of each PDF provides insight into sensitivity to secondary parameters such as air–fuel ratio and ignition voltage: narrower distributions denote robust operating regions where torque remains relatively insensitive to variations in λ and spark energy, while wider distributions signal heightened susceptibility to combustion instability [54]. In particular, the broader tails observed on the low

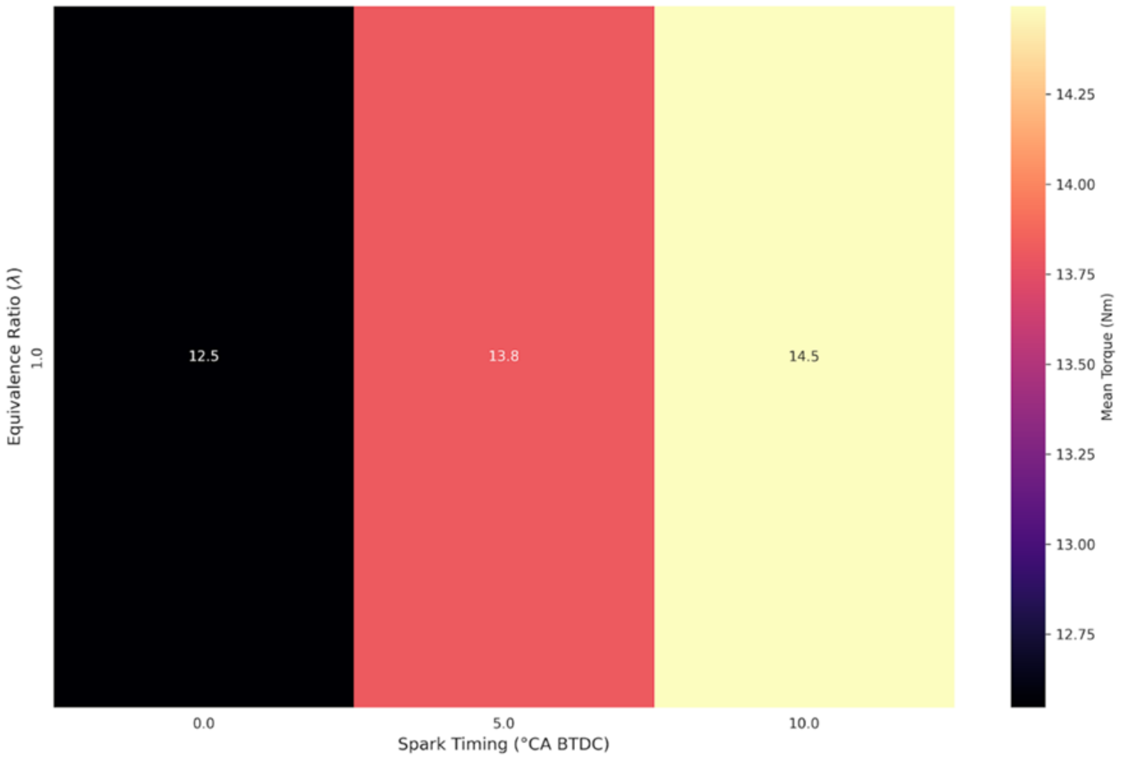

Figure 7. The heatmap showing the causal relation among sparm timing, equivalence ratio, and mean torque

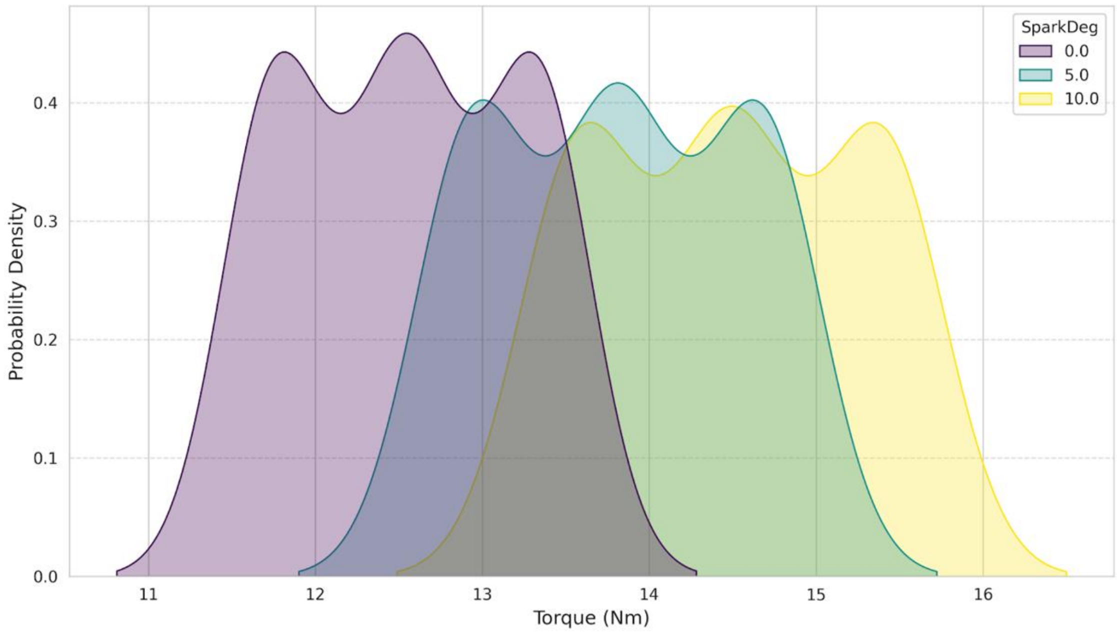

Figure 8. Probability density distribution of engine torque at different spark timing settings (0°, 5°, and 10° BTDC)

torque side correspond to lean-mixture or low-voltage conditions, where incomplete or slowed combustion reduces the pressure rise and increases the likelihood of partial-burn cycles [55]. Collectively, the PDFs illustrate that while advanced spark timing increases mean torque, the stability of the torque output is strongly influenced by mixture strength and ignition quality. These statistical trends reinforce the conclusion that peak engine performance is achieved near the 8°-10° BTDC window, where both the mean torque and distribution sharpness indicate favorable and stable combustion characteristics [56].

The heatmap (**Figure 7**) identifies where maximum torque occurs, showing the MBT region where combustion phasing aligns best with piston motion. Meanwhile, the torque PDFs (**Figure 8**) reveal how stable each region in the heatmap, as advancing timing toward MBT shifts the distributions to higher torque with reduced spread. This indicates better repeatability and lower misfire risk under mixture or ignition fluctuations [6]. Thus, the heatmap defines the optimal operating point, while the PDFs evaluate its reliability. Together, they show that effective calibration must target not only high torque but also minimal variability in hydrogen combustion [57].

The results collectively demonstrate that hydrogen-engine performance in the converted spark-ignition platform is governed almost exclusively by combustion phasing, a dominance stemming directly from hydrogen fundamental properties its high flame speed, low ignition energy, and minimal quenching distance. This primacy is consistently reproduced across all model outputs, from parameter-sensitivity rankings to interpolations, BSFC trends, heatmaps, and torque probability distributions. The Markov-chain model key success lies in probabilistically capturing the nonlinear cascade initiated by spark timing which reveals it as the single most influential parameter exerting decisive leverage over the early kernel development and subsequent flame propagation that dictate torque, efficiency, and fuel consumption. This is evident not only in the sensitivity ranking (**Figure 3**) bu t also in the precipitous torque rise and BSFC valley around 8°-10° BTDC, the region corresponding to MBT. Here, the model quantifies how even minor phasing advances capitalize on hydrogen's rapid combustion, maximizing work output before expansion cooling dominates. While ignition voltage contributes to combustion stability, its effect remains secondary and contingent, acting primarily to ensure kernel survival in sub-optimal mixtures, as indicated by the moderate R^2 and broad vertical dispersion in **Figure 6**. Engine speed (RPM) exerts only modest influence within the studied range, underscoring that in hydrogen applications, the chemical timescale of combustion often decouples from the mechanical timescale, confirming that cycle-to-cycle combustion behavior not inertial scaling dominates performance variance.

The multidimensional analysis enabled by the Markov-chain framework further deconvolves the interaction effects among spark timing, air–fuel ratio, and ignition strength. The heatmap (**Figure 7**) reveals the constrained structural landscape of the combustion space, identifying a narrow MBT island where torque is maximized and sensitivity to λ becomes highly nonlinear as the mixture shifts from optimal, highlighting hydrogen's narrow flammability limits. The torque PDFs (**Figure 8**) provide the crucial probabilistic counterpart, showing that statistical stability varies significantly across timing settings: advancing the spark not only increases mean torque but also markedly compresses the distribution, yielding more repeatable cycles with fewer low-torque outliers under typical perturbations [58]. This compression occurs because advanced, optimal phasing minimizes the window for cyclic variability to affect the combustion outcome. Together, these results show that the heatmap defines where optimal operation occurs, while the PDFs describe how reliably that performance can be attained.

The stochastic fluctuations represented by the Markov-chain model can be interpreted as a macroscopic manifestation of underlying microscopic combustion processes, particularly variations in the population of reactive radicals such as H, O, and OH, which are highly sensitive to local temperature, mixture composition, and ignition conditions. These radical-level fluctuations influence chain-branching kinetics and flame development, leading to variability in heat release, pressure rise, and combustion phasing that is captured statistically through transitions between engine states in the Markov framework.

However, the transition probabilities defined in the Markov model do not directly correspond to quantum transition probabilities between vibrational and rotational energy states; rather, quantum-level energy transitions determine molecular energy distributions that govern reaction rates and radical formation [59]. The cumulative effect of these molecular and quantum-scale processes propagates to cycle-scale combustion variability, which is effectively represented in a coarse-grained manner by the Markov transition probabilities, linking microscopic energy fluctuations to macroscopic engine performance behavior.

The proposed model in this work was validated by comparing the predictions with established studies that have been experimentally validated listed in in Table 2. Across the referenced works, consistent trends are reported, including the existence of an optimal spark timing region (MBT), the sensitivity of torque and efficiency to combustion phasing, and the secondary influence of parameters such as ignition characteristics and operating conditions. The present model reproduces these same fundamental trends, particularly the identification of the MBT region (8–10° BTDC), the nonlinear torque response to spark timing, and the inverse relationship between BSFC and efficiency, demonstrating strong agreement with experimentally supported findings in the literature. While the proposed framework extends beyond prior approaches by incorporating stochastic variability through a Markov-chain formulation, its alignment with validated deterministic results confirms the physical reliability of the model.

This synergistic deterministic-probabilistic insight uniquely facilitated by the Markov-chain approach demonstrates that optimal hydrogen-engine calibration must be redefined as a dual-objective pursuit: simultaneously targeting (1) high average torque and (2) minimal torque variability. The model identifies that these objectives converge in the same narrow phasing region, but are differentially modulated by secondary parameters like λ and voltage, which affect burn completeness and early-flame robustness. In essence, the model transcends simple prediction by not only identifying the best operating region but also quantifying its operational resilience. This provides a critical tool for control-oriented development, where strategies must manage the inherent trade-offs between peak performance and stable operation in the face of multidimensional variations, a challenge particularly acute for hydrogen due to its elevated sensitivity to mixture preparation and ignition quality. The stochastic nature of the model can be further interpreted through its steady-state distribution, stochastic trajectory, and

Table 2. The comparison of this work with the results of other works

No.	Method	Results	Study
1	1D engine simulation with calibrated hydrogen combustion submodel and experimental-based validation	• Accurate prediction of engine performance • NOx emissions • Efficiency trends • Validated against experimental engine data	[60]
2	CFD simulation with ANN/MLR/RBF modeling for HCNG engine	• Improved torque • Efficiency • Reduced emissions • Strong agreement between simulation and experimental data	[61]
3	CFD + detailed chemical kinetics (KIVA-CHEMKIN coupling)	• Good agreement with experimental cylinder pressure and emissions • Parameter configurations across operating conditions	[62]
4	Experimental + 1D modeling of hydrogen injector characteristics	• Validated flow behavior • Injection dynamics • Identified key parameters affecting hydrogen delivery	[63]
5	CFD simulation + SVM + Genetic Algorithm optimization	• High prediction accuracy (<4% error) with experimental validation • Optimized engine parameters for performance and emissions	[64]
6	Markov-chain + Wiebe hybrid stochastic-deterministic model	• Captures both performance trends and cycle-to-cycle variability • Identifies MBT region (8–10° BTDC) • Probabilistic torque distribution • Stability-performance trade-off	This work

probability landscape. The steady-state distribution π, defined by $\pi P=\pi$, represents the long-term likelihood of the system occupying specific engine states and indicates a tendency toward regions near optimal combustion phasing [65]. The stochastic trajectory evolves smoothly across neighboring states due to the high stay probability, reflecting realistic cycle-to-cycle variations in engine operation [66], [67]. The resulting probability landscape shows that high-probability regions coincide with the MBT zone, confirming that the Markov framework captures both performance trends and combustion variability.

4. Conclusion

This study developed a Markov-chain-based combustion modeling framework that captures the hybrid deterministic–probabilistic behavior of hydrogen spark-ignition engines by integrating a Wiebe heat-release model with a discrete state-transition system. The results identify combustion phasing, controlled by spark timing, as the dominant factor governing torque, efficiency, and fuel consumption, while ignition voltage and engine speed play secondary roles. Scientifically, the study demonstrates that optimal hydrogen engine performance is governed not only by peak efficiency but also by combustion stability, highlighting the importance of coupling deterministic performance with stochastic variability in a unified framework. The model successfully identifies the MBT region and quantifies its probabilistic stability, providing insight into the trade-off between performance and robustness. However, the model relies on simplifying assumptions, including neglecting heat transfer, blow-by effects, and variable specific heat, and uses a single-zone Wiebe approach without detailed chemical kinetics. In addition, transition probabilities are assumed rather than experimentally derived. Future work will focus on incorporating heat transfer models, variable thermodynamic properties, and experimental validation, as well as developing data-driven Markov frameworks to better capture real engine variability and support control-oriented applications.

Acknowledgements

This study if funded by Direktorat Riset dan Pengabdian Masyarakat Universitas Brawijaya (DRPM UB) through hibah penelitian dasar unggulan (PDU) 2025 with grant no.[01046.12/UN10.A0501/B/KS/2025].

Author's Declaration

Authors' contributions and responsibilities

Purnami Purnami: Conceptualization; Methodology; Formal Analysis; Project administration; Funding Acquisition; Writing – original draft., Willy Satrio Nugroho: Conceptualization; Formal analysis; Software; Formal analysis; Writing – review and editing., Lilis Yuliati: Interpretation; Validation; Investigation; Visualization., Fikrul Akbar Alamsyah: Investigation; Resources; Data curation; Visualization., Abdul Mudjib Sulaiman Wahid: Investigation; Resources; Writing – review & editing., ING Wardana: Supervision; Validation.

Funding

This study is funded by Direktorat Riset dan Pengabdian Masyarakat Universitas Brawijaya (DRPM UB) through hibah penelitian dasar unggulan (PDU) 2025 with grant no. [01046.12/UN10.A0501/B/KS/2025].

Availability of data and materials

All data are available from the authors.

Competing interests

The authors declare no competing interest.

Additional information

No additional information from the authors.

References

[1] K. Wróbel, J. Wróbel, W. Tokarz, J. Lach, K. Podsadni, and A. Czerwiński, "Hydrogen Internal Combustion Engine Vehicles: A Review," *Energies*, vol. 15, no. 23, p. 8937, Nov. 2022, doi: 10.3390/en15238937.

[2] P. Purnami, W. Satrio Nugroho, Y. K. Sofi'i, and I. N. G. Wardana, "The impact of sodium lauryl sulfate on hydrogen evolution reaction in water electrolysis," *International Journal of Hydrogen Energy*, vol. 79, pp. 1395–1405, Aug. 2024, doi: 10.1016/j.ijhydene.2024.07.127.

[3] Z. Hammi, N. Labjar, M. Dalimi, Y. El Hamdouni, E. M. Lotfi, and S. El Hajjaji, "Green hydrogen: A holistic review covering life cycle assessment, environmental impacts, and color analysis," *International Journal of Hydrogen Energy*, vol. 80, pp. 1030–1045, Aug. 2024, doi: 10.1016/j.ijhydene.2024.07.008.

[4] P. Purnami, N. Willy Satrio, S. Supriyono, and I. N. G. Wardana, "Digitally controlled organic electrocatalyst for water electrolysis," *International Journal of Hydrogen Energy*, vol. 47, no. 23, pp. 11877–11893, Mar. 2022, doi: 10.1016/j.ijhydene.2022.01.203.

[5] T. Li, X.-G. Yue, M. Qin, and D. Norena-Chavez, "Towards Paris Climate Agreement goals: The essential role of green finance and green technology," *Energy Economics*, vol. 129, p. 107273, Jan. 2024, doi: 10.1016/j.eneco.2023.107273.

[6] Z. Yang, J. Wu, H. Yun, H. Zhang, and J. Xu, "Diagnosis and control of abnormal combustion of hydrogen internal combustion engine based on the hydrogen injection parameters," *International Journal of Hydrogen Energy*, vol. 47, no. 35, pp. 15887–15895, Apr. 2022, doi: 10.1016/j.ijhydene.2022.03.031.

[7] P. P. Brancaleoni, E. Corti, V. Ravaglioli, D. Moro, and G. Silvagni, "Innovative torque-based control strategy for hydrogen internal combustion engine," *International Journal of Hydrogen Energy*, vol. 73, pp. 203–220, Jul. 2024, doi: 10.1016/j.ijhydene.2024.05.481.

[8] Y. Zhou, Q. Ruan, Y. Li, Y. Fan, and D. Chen, "A full in-silico approach for quantifying the effect of intramolecular hydrogen bonds on physicochemical properties," *Journal of Molecular Liquids*, vol. 425, p. 127152, May 2025, doi: 10.1016/j.molliq.2025.127152.

[9] D. N. Rrustemi, L. C. Ganippa, T. Megaritis, and C. J. Axon, "New laminar flame speed correlation for lean mixtures of hydrogen combustion with water addition under high pressure conditions," *International Journal of Hydrogen Energy*, vol. 63, pp. 609–617, Apr. 2024, doi: 10.1016/j.ijhydene.2024.03.177.

[10] D. Saini, M. Talei, Y. Yang, R. D. Sandberg, and J. D. Berry, "Improving low-order modelling of cryogenic hydrogen releases," *International Journal of Hydrogen Energy*, vol. 105, pp. 417–426, Mar. 2025, doi: 10.1016/j.ijhydene.2025.01.148.

[11] V. Y. Plaksin and I. A. Kirillov, "Hydrogen flammability and explosion concentration limits for a wide temperature range," *Journal of Loss Prevention in the Process Industries*, vol. 94, p. 105554, Apr. 2025, doi: 10.1016/j.jlp.2025.105554.

[12] H. Sapra, M. Godjevac, P. De Vos, W. Van Sluijs, Y. Linden, and K. Visser, "Hydrogen-natural gas combustion in a marine lean-burn SI engine: A comparitive analysis of Seiliger and double Wiebe function-based zero–dimensional modelling," *Energy Conversion and Management*, vol. 207, p. 112494, Mar. 2020, doi: 10.1016/j.enconman.2020.112494.

[13] S. Yousefian, G. Bourque, and R. F. D. Monaghan, "Bayesian inference and uncertainty quantification for hydrogen-enriched and lean-premixed combustion systems," *International Journal of Hydrogen Energy*, vol. 46, no. 46, pp. 23927–23942, Jul. 2021, doi: 10.1016/j.ijhydene.2021.04.153.

[14] S. Krebs and C. Biet, "Predictive model of a premixed, lean hydrogen combustion for internal combustion engines," *Transportation Engineering*, vol. 5, p. 100086, Sep. 2021, doi: 10.1016/j.treng.2021.100086.

[15] A. A. Agama *et al.*, "Effect of Graphene Oxide Addition on Spark Ignition Engine Performance and Cycle-to-cycle Variation with Gasoline-ethanol Fuel," *Automotive Experiences*, vol. 9, no. 1, 2026, doi: 10.31603/ae.14237.

[16] B. Enderle, B. Rauch, F. Grimm, G. Eckel, and M. Aigner, "Probabilistic Modeling and Uncertainty Quantification of Detailed Combustion Simulation for a Swirl Stabilized Spray Burner," *Flow, Turbulence and Combustion*, vol. 111, no. 2, pp. 603–640, Aug. 2023, doi: 10.1007/s10494-023-00426-1.

[17] W. Xu, T. Yang, C. Liu, K. Wu, and P. Zhang, "Transient identification of supersonic combustion mode by dynamic-VAE and Markov probabilistic modeling," *Combustion and Flame*, vol. 284, p. 114609, Feb. 2026, doi: 10.1016/j.combustflame.2025.114609.

[18] N. N. Smirnov and V. F. Nikitin, "Modeling and simulation of hydrogen combustion in engines," *International Journal of Hydrogen Energy*, vol. 39, no. 2, pp. 1122–1136, Jan. 2014, doi: 10.1016/j.ijhydene.2013.10.097.

[19] S. Verhelst, "Recent progress in the use of hydrogen as a fuel for internal combustion engines," *International Journal of Hydrogen Energy*, vol. 39, no. 2, pp. 1071–1085, Jan. 2014, doi: 10.1016/j.ijhydene.2013.10.102.

[20] R. Georgescu, C. Pana, N. Negurescu, A.

Cernat, C. Nutu, and C. Sandu, "Aspects of the combustion variability analysis at an automotive engine fuelled with hydrogen," *IOP Conference Series: Materials Science and Engineering*, vol. 1303, no. 1, p. 012017, Mar. 2024, doi: 10.1088/1757-899X/1303/1/012017.

[21] K. Zhang and X. Jiang, "An assessment of fuel variability effect on biogas-hydrogen combustion using uncertainty quantification," *International Journal of Hydrogen Energy*, vol. 43, no. 27, pp. 12499–12515, Jul. 2018, doi: 10.1016/j.ijhydene.2018.04.196.

[22] R. Farzam and G. McTaggart-Cowan, "Hydrogen-diesel dual-fuel combustion sensitivity to fuel injection parameters in a multi-cylinder compression-ignition engine," *International Journal of Hydrogen Energy*, vol. 49, pp. 850–867, Jan. 2024, doi: 10.1016/j.ijhydene.2023.09.124.

[23] D. Cirrone, D. Makarov, C. Proust, and V. Molkov, "Minimum ignition energy of hydrogen-air mixtures at ambient and cryogenic temperatures," *International Journal of Hydrogen Energy*, vol. 48, no. 43, pp. 16530–16544, May 2023, doi: 10.1016/j.ijhydene.2023.01.115.

[24] A. Ghosh, N. M. Munoz-Munoz, and D. A. Lacoste, "Minimum ignition energy of hydrogen-air and methane-air mixtures at temperatures as low as 200 K," *International Journal of Hydrogen Energy*, vol. 47, no. 71, pp. 30653–30659, Aug. 2022, doi: 10.1016/j.ijhydene.2022.07.017.

[25] W. S. Nugroho, P. Purnami, A. M. S. Wahid, and I. N. G. Wardana, "Physics-informed neural network for temperature-dependent gas flow modeling in alkaline electrolyzers," *Applied Thermal Engineering*, vol. 289, p. 129916, Mar. 2026, doi: 10.1016/j.applthermaleng.2026.129916.

[26] J. Xiao *et al.*, "Thermodynamic and heat transfer models for refueling hydrogen vehicles: Formulation, validation and application," *International Journal of Hydrogen Energy*, vol. 52, pp. 172–190, Jan. 2024, doi: 10.1016/j.ijhydene.2023.06.081.

[27] D. Levin and Y. Peres, *Markov Chains and Mixing Times*. Providence, Rhode Island: American Mathematical Society, 2017. doi: 10.1090/mbk/107.

[28] P. Purnami, W. S. Nugroho, W. L. Anggayasti, Y. K. Sofi'i, and I. N. G. Wardana, "Markov decision process for current density optimization to improve hydrogen production by water electrolysis," *Electrochemistry Communications*, vol. 177, p. 107987, Aug. 2025, doi: 10.1016/j.elecom.2025.107987.

[29] A. I. Elwalid, D. Mitra, and T. E. Stern, "A Theory of Statistical Multiplexing of Markovian Sources: Spectral Expansions and Algorithms," in *Numerical Solution of Markov Chains*, Boca Raton: CRC Press, 2021, pp. 223–238. doi: 10.1201/9781003210160-12.

[30] V. Korohodskyi *et al.*, "Development of a three-zone combustion model for stratified-charge spark-ignition engine," *Eastern-European Journal of Enterprise Technologies*, vol. 2, no. 5 (110), pp. 46–57, Apr. 2021, doi: 10.15587/1729-4061.2021.228812.

[31] J. M. Borg and A. C. Alkidas, "On the application of Wiebe functions to simulate normal and knocking spark-ignition combustion," *International Journal of Vehicle Design*, vol. 49, no. 1/2/3, p. 52, 2009, doi: 10.1504/IJVD.2009.024240.

[32] A. Aasen, V. G. Jervell, M. Hammer, B. A. Strøm, H. L. Skarsvåg, and Ø. Wilhelmsen, "Bulk and interfacial thermodynamics of ammonia, water and their mixtures," *Fluid Phase Equilibria*, vol. 584, p. 114125, Sep. 2024, doi: 10.1016/j.fluid.2024.114125.

[33] S. Sudarja, D. Deendarlianto, S. Sukamta, R. K. Adi, F. A. K. Yudha, and R. Arizona, "Experimental investigation of two-phase flow characteristics of nitrogen-CMC solution and nitrogen-XG solution in A 0.8 mm X 0.8 mm square capillary tube in a horizontal position," *Mechanical Engineering for Society and Industry*, vol. 5, no. 2, pp. 542–559, Dec. 2025, doi: 10.31603/mesi.15041.

[34] P. V. Manu, T. R. Navaneeth Kishan, and S. Jayaraj, "Thermodynamic Modelling and Experimental Investigation on a CI Engine Operated with Oxy-Hydrogen Gas as the Secondary Fuel," in *26th National Conference on IC Engines and Combustion (NCICEC)*, 2021, pp. 303–314. doi: 10.1007/978-981-15-5996-9_23.

[35] W. Wijayanti, M. N. Sasongko, and Purnami, "The calorific values of solid and liquid yields consequenced by temperatures of mahogany pyrolysis," *ARPN Journal of Engineering and Applied Sciences*, vol. 11, no. 2, pp. 917–921, 2016.

[36] R. C. Nugroho *et al.*, "Prediction of Performance and Emission of Gasoline Engine Fueled with a Gasoline-Ethanol-Methanol Mixture Using One Dimensional Engine Modelling Based on Engine Test Results," *Automotive Experiences*, vol. 7, no. 3, pp. 525–537, Dec. 2024, doi: 10.31603/ae.12141.

[37] A. Yousefi, H. Guo, S. Dev, S. Lafrance, and B. Liko, "A study on split diesel injection on thermal efficiency and emissions of an ammonia/diesel dual-fuel engine," *Fuel*, vol. 316, p. 123412, May 2022, doi: 10.1016/j.fuel.2022.123412.

[38] E. D. Rokhmawati *et al.*, "Numerical Study on the Effect of Mean Pressure and Loop's Radius to the Onset Temperature and Efficiency of Traveling Wave Termoacustic Engine," *Automotive Experiences*, vol. 3, no. 3, pp. 96–103, Sep. 2020, doi: 10.31603/ae.v3i3.3881.

[39] D. Zhao *et al.*, "Evaluation of the turbulent hot jet flame characteristics for achieving high thermal efficiency of hybrid engine," *Applied Thermal Engineering*, vol. 236, p. 121611, Jan. 2024, doi: 10.1016/j.applthermaleng.2023.121611.

[40] A. J. Mohammed and O. M. Ali, "Influence of hydrogen addition on the performance and emissions of gasoline engine," *Results in Engineering*, vol. 26, p. 105426, Jun. 2025, doi: 10.1016/j.rineng.2025.105426.

[41] L. Cardelli, R. Grosu, K. G. Larsen, M. Tribastone, M. Tschaikowski, and A. Vandin, "Algorithmic Minimization of Uncertain Continuous-Time Markov Chains," *IEEE Transactions on Automatic Control*, vol. 68, no. 11, pp. 6557–6572, Nov. 2023, doi: 10.1109/TAC.2023.3244093.

[42] A. Piano, G. Quattrone, F. Millo, F. Pesce, and A. Vassallo, "Development and validation of a predictive combustion model for hydrogen-fuelled internal combustion engines," *International Journal of Hydrogen Energy*, vol. 89, pp. 1310–1320, Nov. 2024, doi: 10.1016/j.ijhydene.2024.09.407.

[43] J. Chang, H. K. Chan, J. Lin, and W. Chan, "Non-homogeneous continuous-time Markov chain with covariates: Applications to ambulatory hypertension monitoring," *Statistics in Medicine*, vol. 42, no. 12, pp. 1965–1980, May 2023, doi: 10.1002/sim.9707.

[44] P. Purnami, W. S. N, I. P. Tama, W. W, Y. K. Sofi'i, and I. Wardana, "The analytic hierarchy process for the selection of water electrolysis electromagnetic ionization booster," *Electrochimica Acta*, vol. 512, p. 145499, Feb. 2025, doi: 10.1016/j.electacta.2024.145499.

[45] J. A. Caton, "Combustion phasing for maximum efficiency for conventional and high efficiency engines," *Energy Conversion and Management*, vol. 77, pp. 564–576, Jan. 2014, doi: 10.1016/j.enconman.2013.09.060.

[46] M. Ichiyanagi *et al.*, "Combustion Analysis of Ammonia/Gasoline Mixtures at Various Injection Timing Conditions in a High Compression Ratio SI Engine with Sub-Chamber," *Automotive Experiences*, vol. 7, no. 2, pp. 321–332, Sep. 2024, doi: 10.31603/ae.10533.

[47] C. Hardiyanto and P. Prawoto, "Effect of Diethyl Ether on Performance and Exhaust Gas Emissions of Heavy-Duty Diesel Engines Fueled with Biodiesel-Diesel Blend (B35)," *Automotive Experiences*, vol. 6, no. 3, pp. 687–701, Dec. 2023, doi: 10.31603/ae.10311.

[48] R. Soenoko, Purnami, and F. G. Utami Dewi, "Second stage cross flow turbine performance," *ARPN Journal of Engineering and Applied Sciences*, vol. 12, no. 6, 2017.

[49] E. Sangkilang, Sasmoko, W. Wijayanti, and I. Wardana, "The effect of sweet orange peel oil additive on virgin coconut oil combustion characteristic," *International Journal of Mechanical Engineering Technologies and Applications*, vol. 7, no. 1, pp. 51–58, 2026, doi: 10.21776/mechta.2026.007.01.6.

[50] O. Fujiwara and K. Kawamata, "Estimation of Spark Voltage and Spark Length Due to ESD Just before Collision between Charged Metal Spheres Using Measurement Waveforms of Radiated Electric Fields," *IEEJ Transactions on Fundamentals and Materials*,

vol. 145, no. 3, pp. 66–75, Mar. 2025, doi: 10.1541/ieejfms.145.66.

[51] S. Saifullo, M. A. Batutah, A. Rizaly, P. Ponidi, H. Kusnanto, and I. Sofana, "Analysis of braking system on energy saving cars 'Sakera' mechanical engineering work, UM Surabaya," *International Journal of Mechanical Engineering Technologies and Applications*, vol. 5, no. 1, pp. 1–11, Jan. 2024, doi: 10.21776/MECHTA.2024.005.01.1.

[52] A. Nugroho, M. J. Winanto, I. Syafa'at, and R. D. Ratnani, "Performance diesel dual fuel engine on additional coconut shell oil," *International Journal of Mechanical Engineering Technologies and Applications*, vol. 4, no. 2, pp. 144–153, Jun. 2023, doi: 10.21776/mechta.2023.004.02.4.

[53] H. Delbari, S. Munshi, and G. McTaggart-Cowan, "Characterizing injection and ignition of hydrogen and hydrogen-methane blend fuels in a static combustion chamber," *Fuel*, vol. 381, p. 133562, Feb. 2025, doi: 10.1016/j.fuel.2024.133562.

[54] A. Firdiansyah, N. Ilminnafik, A. Triono, and M. N. Kustanto, "Effect of Biodiesel B100 and Ethanol Blends on the Performance of Small Diesel Engine," *International Journal of Mechanical Engineering Technologies and Applications*, vol. 2, no. 2, p. 101, Jul. 2021, doi: 10.21776/mechta.2021.002.02.3.

[55] H. Meng, C. Ji, G. Xin, J. Yang, K. Chang, and S. Wang, "Comparison of combustion, emission and abnormal combustion of hydrogen-fueled Wankel rotary engine and reciprocating piston engine," *Fuel*, vol. 318, p. 123675, Jun. 2022, doi: 10.1016/j.fuel.2022.123675.

[56] S. Guo, H. Meng, Q. Zhan, C. Ji, and D. Wang, "In-depth analysis of the key combustion parameters in the hydrogen-fueled Wankel rotary engine," *International Journal of Hydrogen Energy*, vol. 100, pp. 58–66, Jan. 2025, doi: 10.1016/j.ijhydene.2024.12.325.

[57] Y. Qiang *et al.*, "Optimization of power performance and combustion stability of ultra-lean combustion in hydrogen fuel engines through combined turbulent jet ignition and variable valve timing," *Fuel*, vol. 381, p. 133493, Feb. 2025, doi: 10.1016/j.fuel.2024.133493.

[58] C. Park, Y. Kim, S. Oh, J. Oh, and Y. Choi, "Effect of the operation strategy and spark plug conditions on the torque output of a hydrogen port fuel injection engine," *International Journal of Hydrogen Energy*, vol. 46, no. 74, pp. 37063–37070, Oct. 2021, doi: 10.1016/j.ijhydene.2021.08.229.

[59] W. S. Nugroho, P. Purnami, F. A. Alamsyah, A. M. S. Wahid, and I. N. G. Wardana, "Analytical model for magnetic field assisted proton exchange membrane water electrolysis," *Journal of Power Sources*, vol. 661, p. 238694, Jan. 2026, doi: 10.1016/j.jpowsour.2025.238694.

[60] R. Novella, J. Gomez-Soriano, D. González-Domínguez, and O. Olaciregui, "Optimizing hydrogen spark-ignition engine performance and pollutants by combining VVT and EGR strategies through numerical simulation," *Applied Energy*, vol. 376, p. 124307, Dec. 2024, doi: 10.1016/j.apenergy.2024.124307.

[61] J. Zareei, A. Rohani, and W. M. F. Wan Mahmood, "Simulation of a hydrogen/natural gas engine and modelling of engine operating parameters," *International Journal of Hydrogen Energy*, vol. 43, no. 25, pp. 11639–11651, Jun. 2018, doi: 10.1016/j.ijhydene.2018.02.047.

[62] Y. Wang, X. Zhang, C. Li, and J. Wu, "Experimental and modeling study of performance and emissions of SI engine fueled by natural gas–hydrogen mixtures," *International Journal of Hydrogen Energy*, vol. 35, no. 7, pp. 2680–2683, Apr. 2010, doi: 10.1016/j.ijhydene.2009.04.048.

[63] B. Sun, D. Zhang, and F. Liu, "Investigation of the characteristics of hydrogen injector using experiment and simulation in hydrogen internal combustion engine," *International Journal of Hydrogen Energy*, vol. 37, no. 17, pp. 13118–13124, Sep. 2012, doi: 10.1016/j.ijhydene.2012.03.169.

[64] J. Zareei and A. Rohani, "Optimization and study of performance parameters in an engine fueled with hydrogen," *International Journal of Hydrogen Energy*, vol. 45, no. 1, pp. 322–336, Jan. 2020, doi: 10.1016/j.ijhydene.2019.10.250.

[65] T. Wang and P. Plecháč, "Steady-State Sensitivity Analysis of Continuous Time

Markov Chains," *SIAM Journal on Numerical Analysis*, vol. 57, no. 1, pp. 192–217, Jan. 2019, doi: 10.1137/18M119402X.

[66] S. Meyn, R. L. Tweedie, and P. W. Glynn, *Markov Chains and Stochastic Stability*. Cambridge University Press, 2009. doi: 10.1017/CBO9780511626630.

[67] O. R. N. Loasana, M. Iqbal, S. Soeparman, and L. Yuliati, "Performance modeling of PLTU Paiton 1 with variations in main steam pressure, temperature, and condenser pressure using gatecycle," *International Journal of Mechanical Engineering Technologies and Applications*, vol. 7, no. 1, pp. 69–76, 2026, doi: 10.21776//mechta.2026.007.01.8.